https://doi.org/10.30799/jnst.135.18040411 J. Nanosci. Tech. - Volume 4 Issue 4 (2018) 443–446

Share Your Innovations through JACS Directory

Journal of Nanoscience and Technology

Visit Journal at http://www.jacsdirectory.com/jnst

ISSN: 2455-0191

Synthesis and Photocatalytic Studies of Fe_3O_4 Nanoparticles

P. Durga Prasad, P. Siva Prasada Reddy, Atnafu Guadie Assefa, V. Tejeswara Rao, G. Nageswara Rao*

Department of Inorganic and Analytical Chemistry, School of Chemistry, Andhra University, Visakhapatnam – 530 003, Andhra Pradesh, India.

ARTICLE DETAILS

Article history:
Received 01 July 2018
Accepted 12 July 2018
Available online 22 July 2018

Keywords:
Fe_3O_4 Nanoparticles
X-Ray Diffraction
Particle Size Analysis
Methylene Blue (MB)

ABSTRACT

Advances in nanoscience and nanotechnology are centered in the control of size and shape of nanoparticles, as well as attainment of the extended arrangement of nanoparticles in different structures. One dimensional nanostructured magnetic materials are interesting because of their enhanced magnetic properties and potential applications such as information storage and gas sensor. The advanced electronic applications of Fe_3O_4 magnetic nanomaterials are considered to require improvement in the powder processing, particularly, meticulous particle control in the nanometer range and phase purity. Structural properties of Fe_3O_4 nanoparticles were synthesized via sol-gel protocol, the morphology and particles size were determined by X-ray diffraction, scanning electron microscope, transmission electron microscope, energy dispersive X-ray, UV- diffuse reflectance spectrophotometer and particle size analyzer. The structure of as prepared Fe_3O_4 nanoparticles was used for photocatalytic applications.

1. Introduction

Nanomaterials are the most challenging areas of current scientific and technological research because of their tremendous possibilities in novel shapes, structures and the unusual phenomena associated with materials. The field of nanotechnology is one of the most popular areas for current research and development in all technical disciplines. Nanostructured II–VI semiconductors have been studied very intensively in recent time due to their industrial implementation in nanoelectronic devices [1]. The n-type metal oxide semiconductor gas sensors are popular for monitoring caused by toxic and inflammable gases. They exhibit changes in electrical resistance in the presence of toxic and inflammable gases in the ambient atmosphere. The basis of this change in resistance lies in the reaction between the adsorbed oxygen on the oxide surface and a reducing gas, thus causing a decrease in resistance by releasing electrons back into the oxide [2].

Nanostructures of metal oxides have great attention due to their unique properties in novel applications. The devices based on inorganic materials such as metal oxide semiconductors, which works on principle of the change in conductivity with interaction of molecules [3]. Metal oxides nanostructures offer functionality from electrically conducting to insulating and from highly catalytic to inert propertites. One-dimensional nanostructured materials have attracted great attention over the past decade because of their important and often exhibit novel applications such as magnetic, electrical and optical properties. The unique and novel size dependent properties of magnetic oxides have initiated current worldwide intense research on magnetic nanomaterials [4].

Magnetic particles with sizes in the nanometer scale are now of interest because of their many technological applications and unique magnetic properties which differ considerably from those of bulk materials. Below a critical size, magnetic particles become single domain in contrast with the usual multi domain structure of the bulk magnetic materials exhibiting unique phenomena such as super paramagnetic and quantum tunneling of the magnetization [5].

Iron oxides are one of the most important transition metal oxides of technological importance [6]. Fe_3O_4 is a traditional magnetic material used in wide variety of applications such as electronic ignition systems, generators, vending machines, medical implants, wrist watches, inductor core, transformer circuits, magnetic sensors and recording equipment, telecommunications, magnetic fluids, microwave absorbers and other high-frequency applications [7]. Nanoparticles with novel morphologies and desired compositions have drawn immense attention due to their unique morphology and composition-dependent physicochemical properties and their importance in basic scientific research and potential technology applications [8].

The energy gap (*Eg*) is an important feature of semiconductors which determines their applications in optoelectronics [9-12]. The UV-Vis absorption spectroscopy is frequently used to characterize semiconductors materials [13], it is easy to extract the *Eg* values from their absorption spectra knowing their thickness. However, in colloidal samples, the scattering effect is enhanced since more superficial area is exposed to the light beam. In normal incidence mode, dispersed light is counted as absorbed light and the technique does not distinguish between the two phenomena. On the other hand, it is common to obtain powdered materials, frequently UV-Vis absorption spectroscopy is carried out dispersing the sample in liquid media like water, ethanol or methanol. If the particle size of the sample is not small enough, it precipitates and the absorption spectrum is even more difficult to interpret. In order to avoid these complications, it is desirable to use diffuse reflectance spectroscopy (DRS), which enables to obtain *Eg* of un-supported materials [14]. The theory which makes possible to use DRS was proposed by Kubelka and Munk [15].

2. Experimental Methods

2.1 Synthesis of Fe_3O_4 Nanoparticles

During the sol-gel protocol of iron nanoparticles, 3.2 g of poly ethylene glycol (PEG) taken in 25 mL of distilled water and stirred for 30 min. Later 3.3 g of $FeSO_4.7H_2O$ in 10 mL of distilled water, 9.6 g of $Fe_2(SO_4)_3$ in 20 mL of distilled water are stirred separately. Now both $FeSO_4.7H_2O$ and $Fe_2(SO_4)_3$ solutions were added drop by drop into the poly ethylene glycol solution. Then the solution was stirred for 30 min, ammonia solution is added to maintain pH-10. The mixture was further stirred for 4 h and filtered, washed with distilled water and finally rinsed with acetone and dried in hot air oven at 60 °C for 8 h. The dried compound was calcined at different temperatures at 400 °C, 600 °C and 800 °C for 4 h to get Fe_3O_4 nanoparticles.

2.2 Characterization Techniques

X-ray powder diffraction data were recorded on Siemens (D5000) diffractometer using CuKα radiation (λ = 1.5406 Å) in the range of 2θ = 2–65°. Particle size was recorded by particle size analyzer Horiba SZ100. The

*Corresponding Author:gollapallinr@yahoo.com(Gollapalli Nageswara Rao)

https://doi.org/10.30799/jnst.135.18040411

Cite this Article as: P. Durga Prasad, P. Siva Prasada Reddy, Atnafu Guadie Assefa, V. Tejeswara Rao, G. Nageswara Rao, Synthesis and photocatalytic studies of Fe_3O_4 nanoparticles, J. Nanosci. Tech. 4(4) (2018) 443–446.

morphological analysis of the samples was done by using transmission electron microscope (TEM). A drop of the reaction mixture was placed over carbon-coated copper grids and the solvent was allowed to dry. Images were acquired on a Philips Technai-FE 12 TEM (120 kV). The energy dispersive X-ray spectroscopy (EDX) analysis was performed by scanning electron microscopy (SEM) with a Model S520 (Hitachi, Japan) equipped with an EDX detector (Oxford LINK-ISIS 300). The EDX spectrum was measured at 10 kV accelerating voltage.

3. Results and Discussion

3.1 X-Ray Powder Diffraction

XRD patterns of Fe_3O_4 nanoparticles as-synthesized and calcined at different temperatures at 400 °C, 600 °C and 800 °C. From the patterns of samples, it was found that all the different peaks at (110), (024), (116) corresponds to 36°, 48°, 54°. For calcined samples we observed peaks (104), (110), (024), (116) corresponds to 30°, 36°, 48°, 54° to the inverse cubic spinel structure of Fe_3O_4. In the above spectra phase identification is one of the most important uses in XRD.

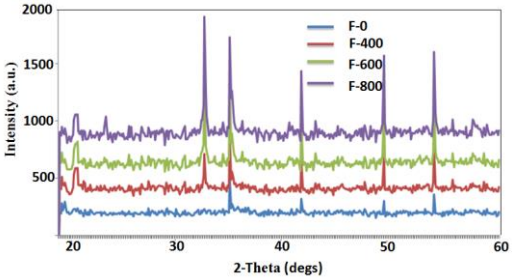

Fig. 1 XRD pattern of a) as- synthesized and (b-d) annealed at different temperatures of Fe_3O_4 nanoparticles

As shown in Fig. 1, XRD pattern of iron nanoparticles after annealing the XRD patterns well indexed to the cubical spinel phase of magnetite and no other peaks observed in as-synthesized material.

3.2 UV-DRS

The UV-DRS spectra of the composites, recorded in the %reflectance mode between 350 to 800 nm are shown in Fig. 2. The optical band gap energy (Eg) is determined for direct and/or indirect band gap. The UV-DRS spectra of the iron nanoparticles, recorded in the %reflectance mode between 350 to 800 nm are shown in Fig. 2. Reflectance band edge of the as synthesized and different annealing temperature of the iron nanoparticles show broad absorption slopes implying the presence of multiple phases in the bulk. The optical band gap energy (Eg) for direct and/or indirect band gap materials are related to the linear absorption coefficient (α) near the absorption edge which is expressed as: $\alpha h\nu = C1(h\nu - Eg)^{1/2}$ and $\alpha h\nu = C2(h\nu - Eg)^2$, respectively. Fig. 3 depicts the Kubelka-Munk transformed reflectance spectra for both the direct and indirect cases of transitions.

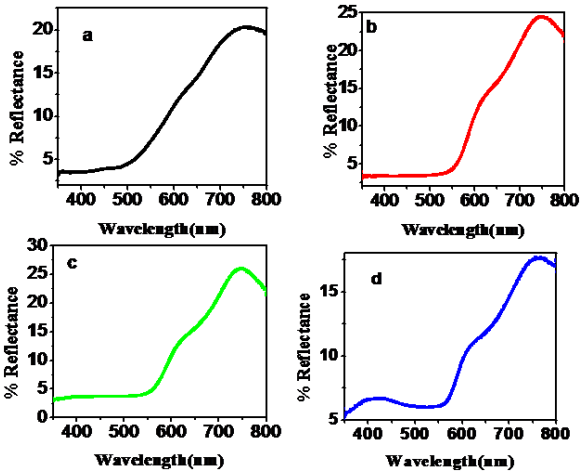

Fig. 2 Representative Diffused reflectance UV-Vis spectra of the iron nanoparticles collected in the reflectance mode

From Fig. 3 the optical band gap (Eg) from the $[F(R).h\nu]^{1/2}$ versus photon energy (hν) plot was estimated to ~2.52, 2.25, 2.25 and 2.3 eV for as-synthesized, F-400, F-600 and F-800 respectively which matches excellently with the reported values of iron nanoparticles a direct band gap semiconductor.

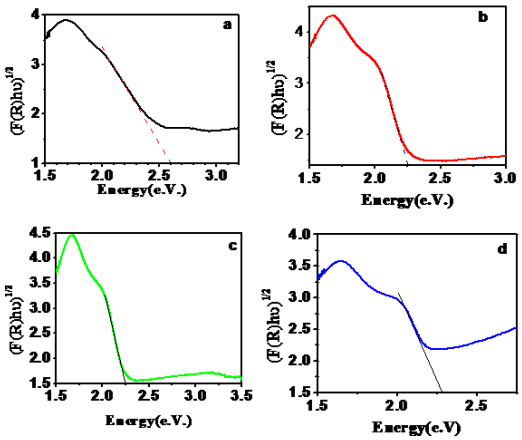

Fig. 3 Kubelka-Munk remission functions, $[F(R).h\nu]^{1/2}$ plotted as a function of photon energy to estimate the optical band gap in direct transition

From the Fig. 4 the optical band gap (Eg) from the $[F(R).h\nu]^2$ versus photon energy (hν) plot (Inset (a)) was estimated to ~ 2.4, 2.2, 2.2 and 2.25 eV for as-synthesized, F-400, F-600 and F-800 respectively which matches excellently with the reported values of iron nanoparticles indirect band gap semiconductor.

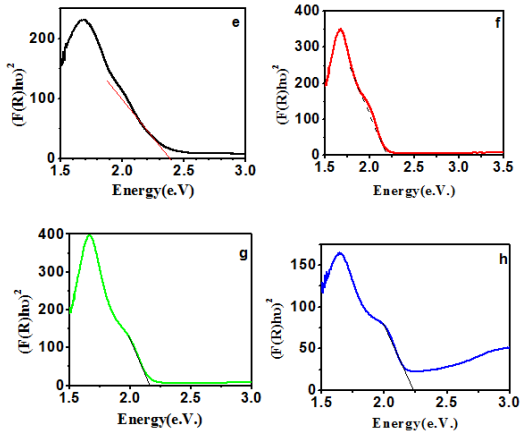

Fig. 4 (e-h) Kubelka-Munk remission functions, $[F(R).h\nu]^2$ plotted as a function of photon energy to estimate the optical band gap in indirect transition

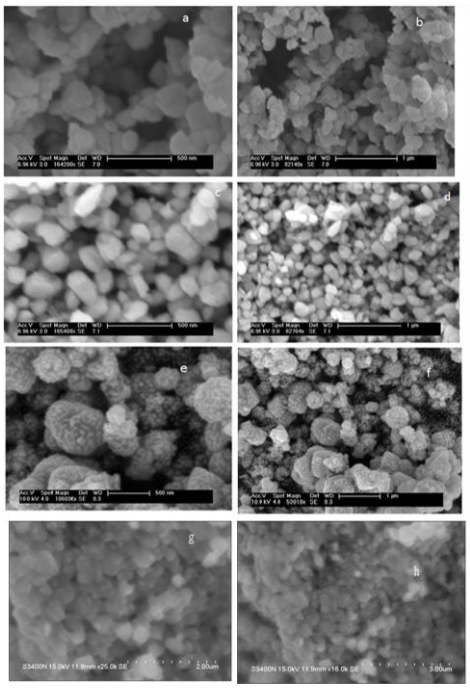

Fig. 5 SEM Images of (a,b) iron nanostructures as-synthesized and calcinated at different temperatures of (c, d) 400 °C, (e, f) 600 °C and (g, h) 800 °C

https://doi.org/10.30799/jnst.135.18040411

Cite this Article as: P. Durga Prasad, P. Siva Prasada Reddy, Atnafu Guadie Assefa, V. Tejeswara Rao, G. Nageswara Rao, Synthesis and photocatalytic studies of Fe_3O_4 nanoparticles, J. Nanosci. Tech. 4(4) (2018) 443–446.

3.3 Scanning Electron Microscope Study

Scanning electron microscopy (SEM) was performed to examine the morphology and structure of the as-synthesized and different annealing temperature materials such as F-400, F-600 and F-800. The morphological structures of the material are clearly seen from Figs. 5a and b are as-synthesized materials which are appeared like thin flakes of nano structures. Figs. 5c and d shows dumbbells and peanut like morphological nano structures obtained at 400 °C calcination. Figs. 5e and f are illustrates flower/bouquet like morphology are seen when the samples are at the calcined at 600 °C and Figs. 5g and h illustrates small spheroids which are obtained at 800 °C calcination temperature.

3.4 EDAX Pattern of Synthesized Iron Nanostructures

Fig. 6 represents the compositional analysis of iron nanoparticles under the energy dispersive X-ray analysis (EDX). The EDX spectrum confirms the presence of Fe, O signal in the sample without any other impurities, strongly indicates the high purity of the final product obtained.

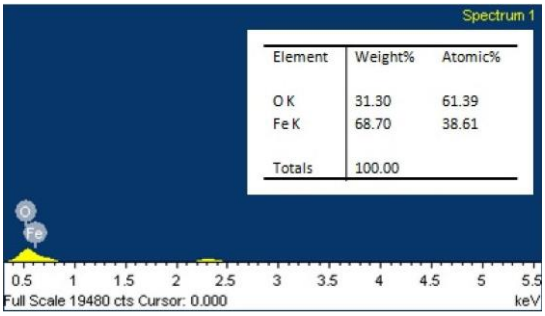

Fig. 6 EDAX pattern of synthesized iron nanostructures

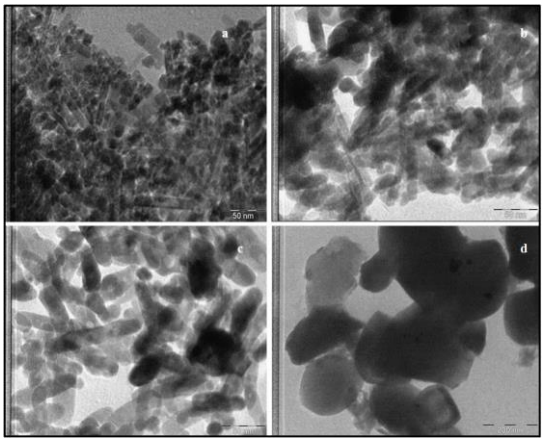

Fig. 7 TEM images of (a) iron nanoparticles as-synthesized and calcinated at different temperatures at (b) 400 °C, (c) 600 °C and (d) 800 °C

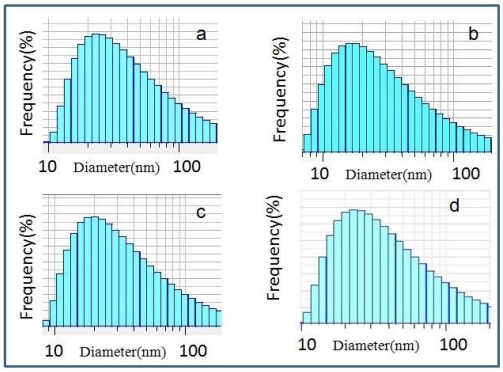

Fig. 8 a) corresponds as –synthesized, b) F-400, c) F-600 and d) F-800 of Fe_3O_4 nanoparticles

3.5 TEM Analysis

Transmission electron microscopy (TEM) was performed to examine the morphology and structure of the as-synthesized and different annealing temperature materials such as F-400, F-600 and F-800 and shown in Fig. 7. As-synthesized materials are in rod shape structure attached with spherical particles due to agglomeration, at 400 °C calcined sample has complete nanorod structures and sample at 600 °C calcined also illustrates nanorod structures and finally at 800 °C calcined sample has completely changes the structure of the sphere shape nanoparticles. From this we can say that particle size varies towards annealing temperature.

3.6 Particle Size Analysis

Particle size distribution of Fe_3O_4 nanoparticles are shown in the Fig. 8 as-synthesized and calcined between 400-800 °C. It is observed that as-synthesized sample as per average particle size of 11 nm and calcined at 800 °C as average particles size of 23 nm. It is also seen that particle size increases with increase in calcination temperature.

3.7 Photocatalytic Application

The photocatalytic performances of Iron nanoparticles were demonstrated by room temperature UV-light degradation of MB. In a typical photocatalytic reaction 20 mg of iron nanoparticles was ultrasonically dispersed in a 20 mL of aqueous MB (1 x 10^{-5} M) in a quartz reactor. The solution was magnetically stirred for 30 minutes in dark to saturate the adsorption/desorption of MB solution on catalyst. After 30 minutes of stirring the solution was irradiated with UV light accompanied by proper stirring to ensure uniform exposure of the suspension throughout the process. The reactor temperature is maintained low by circulating cold water. At periodic time interval 1.5 mL of aqueous MB solution was collected from the photo reactor and centrifuged to separate out any inorganic particles and the UV absorption was recorded. The degradation of MB was monitored by observing the characteristic absorption peak of MB at about 660 nm.

In the present study, we have maintained different pH of methylene blue (MB) dye which are pH-3, pH-7 and pH-10. The four samples are run for four hours with different pH values. During the pH-3 and pH-7 the samples carried for four hours and in pH-10 with in 15 min total degradation was completed. During the pH-3 sample F4-pH3-4H has faster degradation than other samples which shown in Fig. (9a) and during the pH-7 sample F4-pH7-4H has faster degradation than other samples which shown in Fig. (9b) and finally during the pH-10 sample F4-pH10-15M degradation is faster than other samples as shown in (9c) which were shown below Fig. 9.

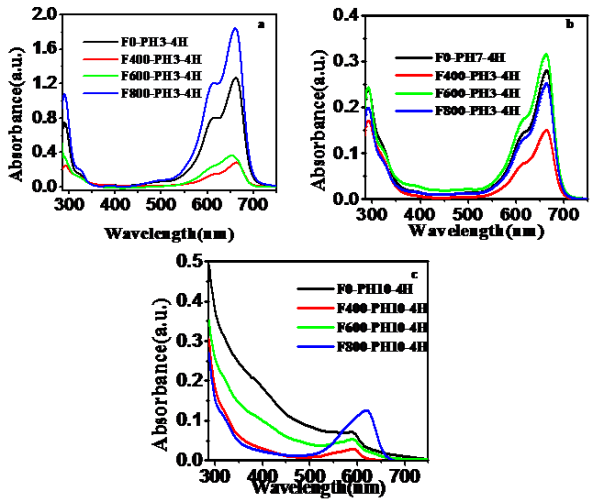

Fig. 9 UV–visible spectroscopic changes of the aqueous MB solution in the presence of as-synthesized and calcined at different temperature in the presence of iron nanoparticles at different PH concentrations a) pH-3, b) pH-7 and c) pH-10.

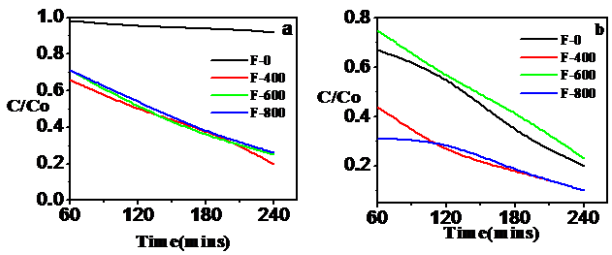

Fig. 10 UV–visible spectroscopic changes of photocatalytic degradation

The UV-spectra clearly shows the peak at λ max of 660 nm gradually decreasing with increasing illumination time indicating that the MB undergoes an obvious degradation with time. Fig. 10 depicts the approximate linear relationship of C/C_o versus the irradiation time t. It can

https://doi.org/10.30799/jnst.135.18040411

Cite this Article as: P. Durga Prasad, P. Siva Prasada Reddy, Atnafu Guadie Assefa, V. Tejeswara Rao, G. Nageswara Rao, Synthesis and photocatalytic studies of Fe_3O_4 nanoparticles, J. Nanosci. Tech. 4(4) (2018) 443–446.

be expressed as follows: $\ln(C/C_o) = kt$, where k is the degradation reaction rate constant, C_o and C are the initial concentration and the concentration at reaction time t for MB, respectively and the results are displayed in Fig. 10. The apparent decomposition rate constants as the evidence for the raspberry nanoparticles assembled found to be MB/iron nanoparticles suspensions were irradiated for 350 nm. The sample with the largest rate constant has the highest catalytic activity. The experimental results reveal the superior photocatalytic performances of F-400 material.

Generally, the photocatalytic efficiency of semiconductors is mainly dependent on the separation of photo generated electron–hole pairs and the transfer of the separated electrons from the photocatalyst to the organic pollutant. In our study, the sizes of the Iron nanoparticles as a photocatalyst play important roles in improving the photocatalytic performance. The ultrafine nanoparticles are responsible to reduce the recombination opportunities of electron–hole pairs. Nanoparticles assembled spheres are beneficial by increasing the absorption and increasing the number of reaction sites. Hence, the sample calcined at 400 °C shows excellent photocatalytic efficiency towards MB.

4. Conclusion

DRS is more convenient technique to characterize unsupported nanomaterials than UV-Vis absorption spectroscopy, since it takes advantage of the enhanced scattering phenomenon in powder materials. Effects of light scattering in the absorption spectra of powder samples dispersed in liquid media can be avoided using DRS. If the absorption peak is not well resolved, even the use of derivative of absorption spectra does not guarantee the exact estimation of *Eg*, and can lead erroneous conclusions. Finally, the DRS technique does not require a powder sample to be dispersed in any liquid medium, so the material is not contaminated or consumed.

Acknowledgement

The authors gratefully acknowledge to UGC, NEW DELHI for financial assistance and DST-FIST for instrument laboratory, Department of Inorganic and Analytical Chemistry for providing instrumentation facility.

References

[1] A.V. Nabok, B. Iwantono, A.K. Hassan, A.K. Ray, T. Wilkop, Electrical characterization of LB films containing CdS nanoparticles, Mater. Sci. Eng. C 22 (2002) 355-358.
[2] S.K. Biswas, P. Pramanik, Studies on the gas sensing behavior of nanosized $CuNb_2O_6$ towards ammonia, hydrogen and liquefied petroleum gas, Sensor Actuat. B 133 (2008) 449-455.
[3] D.S. Dhawale, D.P. Dubal, V.S. Jamadade, R.R. Salunkhe, S.S. Joshi, C.D. Lokhande, Room temperature LPG sensor based on n-CdS/p-polyaniline heterojunction, Sensor Actuat. B 145 (2010) 205-210.
[4] D. Guin, S.V. Manorama, S. Radha, A.K. Nigam, One-pot size and shape controlled synthesis of DMSO capped iron oxide nanoparticles, Bull. Mater. Sci. 29(6) (2006) 617-621.
[5] Y.L.N. Murthy, I.V.K. Viswanath, T. Kondala Rao, R. Singh, Synthesis and characterization of nickel copper ferrite, Int. J. ChemTech Res. 1(4) (2009) 1308-1311.
[6] M. Mohapatra, S. Anand, Synthesis and applications of nano-structured iron oxides/hydroxides-a review, Int. J. Eng. Sci. Technol. 2(8) (2010) 127-146.
[7] P.M.P. Swamy, S. Basavaraja, L. Arunkumar, N.V.S. Rao, R. Nijagunappa, A. Venkataraman, Synthesis and characterization of zinc ferrite nanoparticles obtained by self-propagating low-temperature combustion method, Bull. Mater. Sci. 34(7) (2011) 1325-1330.
[8] R. Shi, G. Chen, W. Ma, D. Zhang, G. Qiu, X. Liu, Shape-controlled synthesis and characterization of cobalt oxides hollow spheres and octahedral, Dalton Trans. 41 (2012) 5981-5987.
[9] Y.I. Alivov, C. Liu, A. Teke, M.A. Reshchikov, S. Dogan, V. Avrutin, et al., A comprehensive review of ZnO materials and devices, J. Appl. Phys. 98 (2005) 041301-1-103.
[10] D.M. Bagnall, Y.F. Chen, Z. Zhu, T. Yao, Optically pumped lasing of ZnO at room temperature, Appl. Phys. Lett. 70 (1997) 2230-2232.
[11] T. Aoki, Y. Hatanaka, D.C. Look, ZnO diode fabricated by excimer-laser doping, Appl. Phys. Lett. 76 (2000) 3257-3258.
[12] C. Boemare, T. Monteiro, M.J. Soares, J.G. Guilherme, E. Alves, Green and red emission in Ca implanted GaN samples, Phys. B Condensed Matter 308-310 (2001) 42-46.
[13] U. Pal, D. Samanta, S. Ghorai, A.K. Chaudhuri, Optical constants of vacuumevaporated polycrystalline cadmium selenide thin films, J. Appl. Phys. 74 (1993) 6368-6374.
[14] D.G. Barton, M. Shtein, R.D. Wilson, S.L. Soled, E. Iglesia, Structure and electronic properties of solid acids based on tungsten oxide nanostructures, J. Phys. Chem. B 103 (1999) 630-640.
[15] P. Kubelka, F. Munk, A contribution to the appearance of the paint, J. Tech. Phys. 12 (1931) 593-601.

https://doi.org/10.30799/jnst.135.18040411

Cite this Article as: P. Durga Prasad, P. Siva Prasada Reddy, Atnafu Guadie Assefa, V. Tejeswara Rao, G. Nageswara Rao, Synthesis and photocatalytic studies of Fe_3O_4 nanoparticles, J. Nanosci. Tech. 4(4) (2018) 443–446.